

HOUSE OF CARDS: MASSIVE WEIGHTS IN LLMs

Jaehoon Oh, Seungjun Shin, Dokwan Oh

Samsung Advanced Institute of Technology, Korea

{jh0104.oh, sj0216.shin, dokwan.oh}@samsung.com

ABSTRACT

Massive activations, which manifest in specific feature dimensions of hidden states, introduce a significant bias in large language models (LLMs), leading to an overemphasis on the corresponding token. In this paper, we identify that massive activations originate not from the hidden state but from the intermediate state of a feed-forward network module in an early layer. Expanding on the previous observation that massive activations occur only in specific feature dimensions, we dive deep into the weights that cause massive activations. Specifically, we define *top-k massive weights* as the weights that contribute to the dimensions with the top- k magnitudes in the intermediate state. When these massive weights are set to zero, the functionality of LLMs is entirely disrupted. However, when all weights except for massive weights are set to zero, it results in a relatively minor performance drop, even though a much larger number of weights are set to zero. This implies that during the pre-training process, learning is dominantly focused on massive weights. Building on this observation, we propose a simple plug-and-play method called `MacDrop` (**massive weights curriculum dropout**), to rely less on massive weights during parameter-efficient fine-tuning. This method applies dropout to the pre-trained massive weights, starting with a high dropout probability and gradually decreasing it as fine-tuning progresses. Through experiments, we demonstrate that `MacDrop` generally improves performance across zero-shot downstream tasks and generation tasks.

1 INTRODUCTION

Large language models (LLMs), such as GPT (Achiam et al., 2023) and Llama (Touvron et al., 2023; Dubey et al., 2024), have achieved remarkable success across diverse natural language tasks (Roziere et al., 2023; Mitra et al., 2024; Labrak et al., 2024; Wu et al., 2023). Their success is largely attributed to the pre-training phase, during which they are trained on extensive high-quality corpora datasets to predict the next token (Longpre et al., 2024; Zhao et al., 2024; Shen et al., 2023). However, despite the impressive achievements of LLMs, a crucial gap remains in our understanding of the underlying mechanisms that drive their remarkable performance.

Recently, Xiao et al. (2024) uncovered an intriguing phenomenon in LLMs, referred to as *attention sinks*: an unexpectedly large portion of attention is directed toward the initial tokens, regardless of their semantic context, after a small number of early layers. They demonstrated that under a restricted budget, focusing attention solely on recent window leads to poor performance, and that performance is recovered when initial tokens are included. Based on this observation, they proposed StreamingLLM, which retains the key-value caches of the initial sink tokens and the recent tokens for streaming use of LLMs. Yu et al. (2024) further investigated the attention sinks phenomenon, finding that attention sinks can appear both in the initial tokens and in later tokens with less semantic importance (e.g., ‘.’ and ‘\n’). They showed that when sink tokens appear later in a sequence, sink tokens can potentially result in performance degradation. Inspired by this observation, they proposed a head-wise attention calibration technique without requiring additional training. Concurrently, Sun et al. (2024) discovered the existence of *massive activations* in the hidden states of LLMs, with magnitudes substantially larger than the others. Massive activations are jointly identified based on their sequence and feature dimensions within the hidden states. Specifically, massive activations occur at the initial tokens and weak semantic tokens according to the model, and are consistently present in only a few fixed feature dimensions. Moreover, they connected massive activations with attention sinks, suggesting that massive activations inject implicit bias into the self-attention mechanism throughout the pre-training phase.

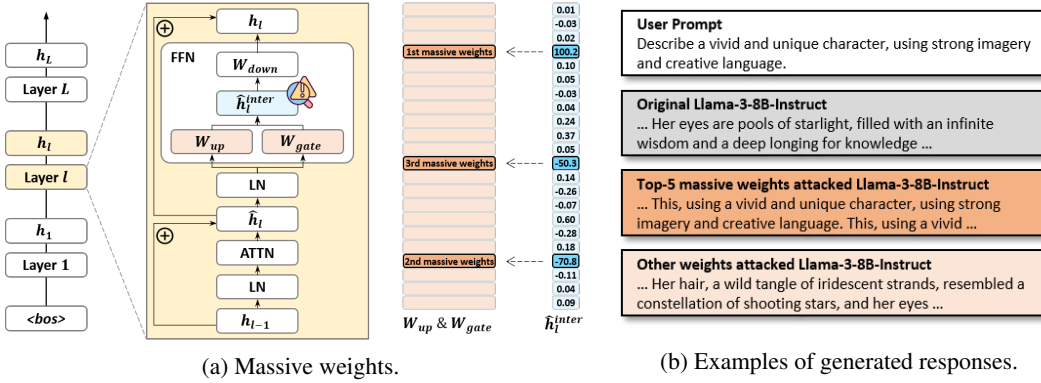


Figure 1: (a) Massive weights are defined as the rows of \mathbf{W}_{gate} and \mathbf{W}_{up} in a specific layer l using the *bos* token, which produce the top- k magnitudes of the intermediate state \hat{h}_l^{inter} . Because massive weights are defined within a single layer l , the ratio of massive weights is significantly low compared to the overall number of parameters. For instance, in the case of Llama-3-8B, the proportion of top-5 massive weights is 0.0005% of the model’s total parameters. (b) When the top-5 massive weights are zeroed out, instruction-tuned LLMs completely lose their ability to generate text. On the other hand, when only the top-5 massive weights remain unchanged in \mathbf{W}_{gate} and \mathbf{W}_{up} , instruction-tuned LLMs retain their generation capability.

In this paper, we first delve deeper into massive activations, providing two key observations. (1) The *bos* token always has massive activations in the same feature dimensions and makes attention sinks, regardless of its position in the sequence. This observation enables us to focus only on the feature dimensions, instead of both the sequence and feature dimensions, when addressing massive activations. Namely, a simplified and consistent analysis of massive activations can be achieved by using only the *bos* token. (2) Massive activations originate in the intermediate state \hat{h}_l^{inter} within an early layer l , before appearing in the hidden state h_l , as illustrated in Figure 1(a). Namely, massive activations triggered in \hat{h}_l^{inter} are subsequently and continuously propagated through skip connections. This observation implies that the feed-forward network in layer l plays a crucial role in LLMs.

Next, we shift our focus from activations to the weights, relying on the fact that massive activations consistently appear in the same feature dimensions. In detail, we define the *top- k massive weights* as the rows of \mathbf{W}_{up} and \mathbf{W}_{gate} in the feed-forward network at layer l that produce the top- k magnitudes of the intermediate state \hat{h}_l^{inter} , as illustrated in Figure 1(a). It is important to note that massive weights, defined within a single layer l , account for a substantially small fraction compared to the model’s total parameters. This holds true even when compared to the entire \mathbf{W}_{up} and \mathbf{W}_{gate} . Nevertheless, massive weights are crucial factors that can completely influence the performance of LLMs. Figure 1(b) presents the generated responses of three models to the given user prompt: original model, top-5 massive weights attacked model, and other weights attacked model. Here, other weights represent all weights in \mathbf{W}_{up} and \mathbf{W}_{gate} at layer l that do not belong to the top-5 massive weights, and an attack sets corresponding weights to zero. When the massive weights are attacked, the model becomes poor and repeats the user prompt. On the contrary, when other weights are attacked, the model does not entirely lose its generation capability, even though a much greater number of weights are set to zero in the same projection matrices. These observations imply that massive weights are dominantly learned during pre-training and highly related to the performance of LLMs.

Finally, we propose a straightforward plug-and-play method during parameter-efficient fine-tuning, named **massive weights curriculum dropout** (MacDrop). This method applies dropout to the pre-trained massive weights, rather than additional trainable weights, starting with a high dropout rate that is progressively reduced throughout the fine-tuning phase. The intuition behind MacDrop is that a high initial dropout rate encourages the model to lessen dependence on the massive weights predominantly learned during the pre-training phase. Then, reducing the dropout rate facilitates a more stable convergence, ensuring the pre-trained model is leveraged with neglectable damage by the end of fine-tuning. In zero-shot downstream tasks and generation tasks, we demonstrate that MacDrop generally enhances model performance.

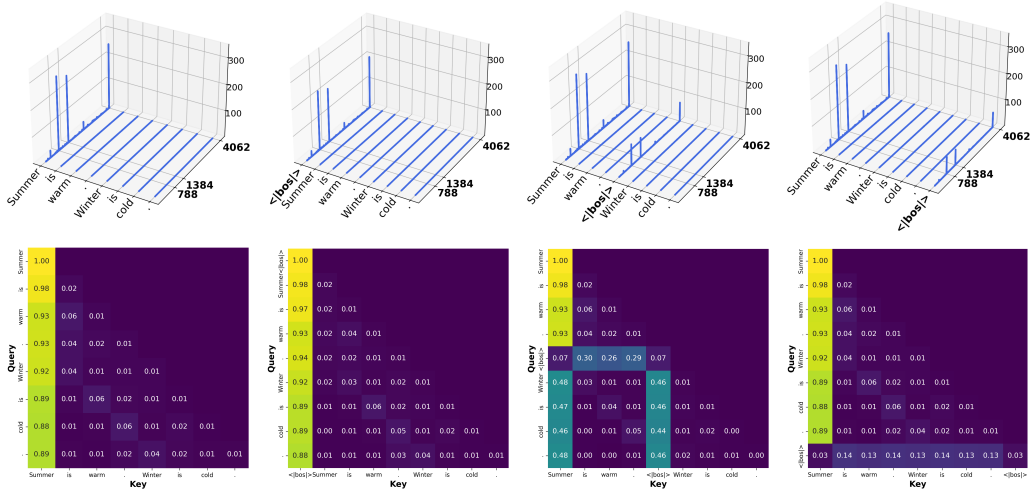


Figure 2: (Top) Magnitudes of the hidden state and (Bottom) attention scores after Softmax, according to the position of the *bos* token. The described hidden state is the output of layer 2 (i.e., h_2). The attention scores are calculated at layer 3 (i.e., after massive activations appear) and averaged across different heads. The *bos* token always has massive activations, regardless of its position.

2 MASSIVE WEIGHTS

In this section, we review the key observations on massive activations reported by Sun et al. (2024) and extend the analysis by exploring various states using the *bos* token, which was not covered. Based on this expanded analysis, we formally define top- k massive weights in a specific layer and investigate their importance through two opposite types of attacks.

2.1 PREREQUISITE: MASSIVE ACTIVATIONS

Autoregressive Transformers (Vaswani et al., 2017) are structured with L decoding layers. Each layer $l \in [1, L]$ includes an attention (ATTN) module and a feed-forward network (FFN) module. These modules are connected via residual connections (He et al., 2016), each following a layer normalization (LN) layer (Ba, 2016). The previous hidden state h_{l-1} is fed into layer l and processed to produce the subsequent hidden state h_l :

$$h_l = \hat{h}_l + \text{FFN}(\text{LN}(\hat{h}_l)), \text{ where } \hat{h}_l = h_{l-1} + \text{ATTN}(\text{LN}(h_{l-1})) \quad (1)$$

Sun et al. (2024) primarily concentrated on the activations within hidden states, identifying that certain activations exhibit exceptionally large magnitudes, which they termed *massive activations*. Massive activations are observed at the starting position (i.e., input-agnostic) or at the delimiter tokens, depending on the model. Furthermore, these activations are confined to a small number of fixed feature dimensions, even within these tokens. These activations initially emerge after passing through several early layers and then decreases as they near the last layer.

Massive activations are strongly tied to the attention sinks phenomenon, as identified by Xiao et al. (2024), in which attention is abnormally concentrated on a small subset of tokens. In detail, a given query state tends to have positive cosine similarity with the key states of the tokens exhibiting massive activations, and negative cosine similarity with those of other tokens. Consequently, attention is heavily skewed toward the tokens associated with massive activations.

2.2 FURTHER ANALYSIS ON MASSIVE ACITVATIONS

We primarily utilize the Llama-3-8B model (Dubey et al., 2024) and explicitly specify other models when necessary.

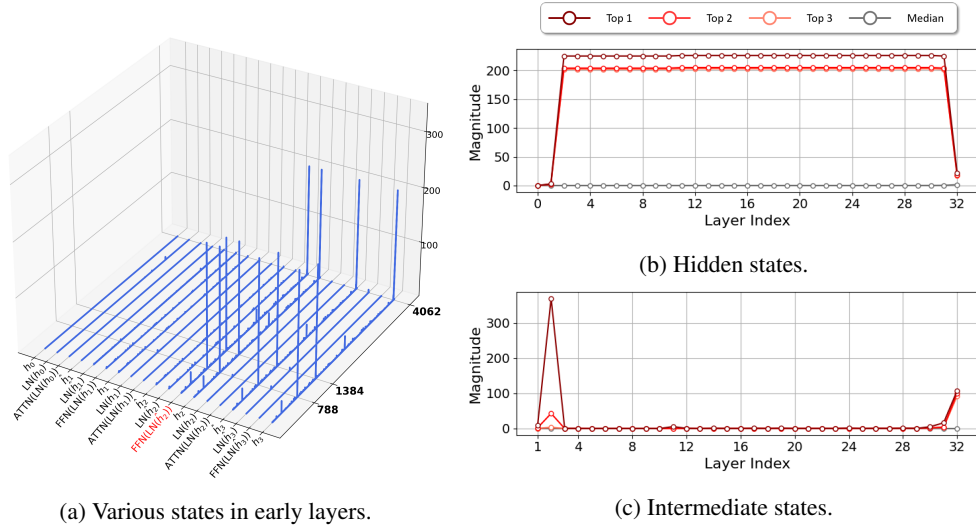


Figure 3: (a) Magnitudes of various states and (b and c) the top three and median magnitudes of hidden states and intermediate states across layers. These results show that massive activations in the hidden state originate from those in the interemmediate state in a FFN module in an early layer.

***bos* token always has massive activations, regardless of its position.** We begin by examining whether any specific token consistently triggers massive activations. As noted by Sun et al. (2024), massive activations are observed when any token is placed in the starting position; however, no single token has been found to trigger massive activations regardless of its position. The existence of such a token would greatly facilitate the analysis and algorithm development for handling massive activations, making the process more deterministic by focusing on that token.

Based on the previous observation that nonsemantic tokens can trigger massive activations in certain LLMs, we focus our analysis on the *bos* token. Figure 2 describes the magnitudes of activations of the hidden state and normalized attention scores according to the position of the *bos* token, after massive activations appear. We use the implementation¹ of massive activations for this example and visualization. Llama-3-8B does not have massive activations at delimiter tokens such as ‘.’ (first column). When the *bos* token is placed in the starting position (second column), the ‘Summer’ token loses its massive activations, while when the *bos* token is placed in the middle or ending position (third and fourth columns), it triggers massive activations in the same feature dimensions (i.e., 788, 1384, and 4062). What is intriguing is that, despite the difference in magnitude according to the position, the *bos* token similarly exhibits attention sinks. Therefore, we use only the *bos* token (placed at the starting position) for the continuation of analysis and algorithm development.

Massive activations originate in the intermediate state of a FFN module. Next, we trace various states in early layers until the first massive activations appear, using the *bos* token. Specifically, we monitor h_{l-1} , $\text{LN}(h_{l-1})$, $\text{ATTN}(\text{LN}(h_{l-1}))$, \hat{h}_l , $\text{LN}(\hat{h}_l)$, and $\text{FFN}(\text{LN}(\hat{h}_l))$ in Eq. (1) throughout early layers. Figure 3(a) illustrates the magnitudes of various states in layers $l \in [1, 3]$. It is observed that $\text{FFN}(\text{LN}(\hat{h}_2))$ has massive activations before h_2 . With Figure 3(b), which describes the top three and median magnitudes of the hidden state¹, it is observed that the massive activations generated within a FFN module at layer 2 are transmitted directly to the next hidden state and then propagated solely through the residual connections.

Furthermore, we decompose a FFN module into $\mathbf{W}_{\text{down}}(\sigma(\mathbf{W}_{\text{gate}}(\cdot)) \odot \mathbf{W}_{\text{up}}(\cdot))$, to analyze the intermediate states (i.e., the output of $\sigma(\mathbf{W}_{\text{gate}}(\cdot)) \odot \mathbf{W}_{\text{up}}(\cdot)$). Figure 3(c) describes the top three and median magnitudes of the intermediate state across layers. It is demonstrated that *massive activations originate in the intermediate state of a FFN module in an early layer l* . This result implies that \mathbf{W}_{up} and \mathbf{W}_{gate} in layer l are closely tied to massive activations. Additional results for other LLMs are provided in the Appendix C.

¹<https://github.com/locuslab/massive-activations>

Table 1: Perplexity and zero-shot downstream tasks performance according to the attack.

Models	WikiText	C4	PG-19	Avg. (\downarrow)	ARC-E	ARC-C	BoolQ	PIQA	WG	Avg. (\uparrow)
Llama-3-8B	5.75	9.94	8.98	8.22	77.4	52.7	81.4	80.8	72.9	73.0
top-5 zeroing	104.57	132.83	130.83	122.74	29.1	22.0	41.8	53.8	50.3	39.4
top-5 retaining	10.15	23.98	28.72	20.95	75.0	48.0	80.2	77.7	74.1	71.0
Llama-3-70B	2.68	7.59	6.02	5.43	85.8	64.2	85.3	84.6	80.5	80.1
top-5 zeroing	11135.81	7288.86	4696.49	7707.05	28.6	22.8	38.0	55.5	49.5	38.9
top-5 retaining	3.47	9.93	7.26	6.89	45.9	25.6	83.9	64.6	77.0	59.4
Llama-3.1-405B (8bit)	1.41	6.20	3.23	3.61	86.3	66.0	88.2	85.0	81.1	81.3
top-5 zeroing	1785.56	985.36	633.40	1134.77	26.6	25.9	37.8	49.7	50.3	38.1
top-5 retaining	2.47	9.36	5.61	5.81	83.0	62.5	83.1	83.2	70.3	76.4

2.3 MASSIVE WEIGHTS

Massive weights are defined based on massive activations in the intermediate state at layer l , denoted as \hat{h}_l^{inter} , when the *bos* token is fed into LLMs. To elaborate, we define the rows in the projection matrix \mathbf{W}_{up} (and \mathbf{W}_{gate} , if it exists) that correspond to the indices of the top- k magnitudes in \hat{h}_l^{inter} as *top- k massive weights*, depicted in Figure 1(a). It is noted that massive weights are defined within one specific layer, which means the number of massive weights is significantly smaller compared to the total number of parameters in LLMs. For example, in Llama-3-8B, the number of top- k massive weights is calculated as $2 \times k \times 4096$, where 4096 represents the dimensions of hidden state. If k is set to 5, massive weights account for approximately 0.0005% of the total parameters in Llama-3-8B, approximately 0.0001% in Llama-3-70B, and approximately 0.00004% in Llama-3.1-405B.

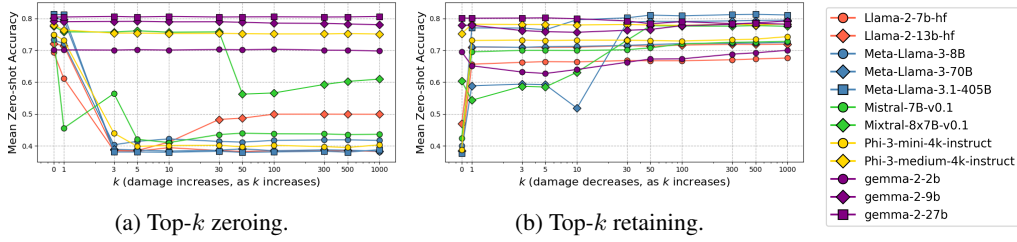
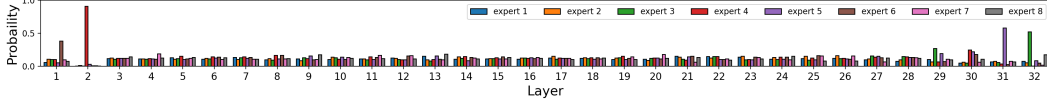
Massive weights are extremely small in quantity, their impact is tremendous. To assess the significance of massive weights, we conduct two types of attacks: top- k zeroing and top- k retaining. Note that these attacks only affect the \mathbf{W}_{up} and \mathbf{W}_{gate} projection matrices in layer l , where massive weights are present. The first attack is to set the top- k massive weights to zero (i.e., darker orange weights in Figure 1(a)). In essence, this attack is very similar to the one proposed in Sun et al. (2024), where massive activations in the hidden state are zeroed out in a single layer. The difference is that their attack targets the hidden state, while our attack targets the intermediate state. The second attack is to set all weights to zero except for top- k massive weights (i.e., lighter orange weights in Figure 1(a)). That is, the number of rows being damaged in each attack is k and the dimensions of intermediate state – k , respectively.

Following Sun et al. (2024), we assess perplexity¹ on three datasets: WikiText (Merity et al., 2017), C4 (Raffel et al., 2020), and PG-19 (Rae et al., 2020). Additionally, we evaluate zero-shot accuracy² on five tasks: Arc-Easy, Arc-Challenge (Clark et al., 2018), BoolQ (Clark et al., 2019), PIQA (Bisk et al., 2020), and WinoGrande (WG) (Sakaguchi et al., 2021). Table 1 presents the results of two attacks on Llama-3-8B, Llama-3-70B, and Llama-3.1-405B (8bit)³, when k is set to 5. Llama-3-8B has its massive weights in layer 2 out of 32 layers, Llama-3-70B in layer 4 out of 80 layers, and Llama-3.1-405B in layer 6 out of 126 layers (Appendix B). The larger the difference from the original performance, the stronger the attack.

Top-5 zeroing is a much stronger attack than top-5 retaining, even though top-5 retaining sets several thousands times more weights to zero compared to top-5 zeroing does for the same projection matrices. This means that in the projections \mathbf{W}_{up} and \mathbf{W}_{gate} at layer l , having only massive weights is significantly better than having all weights except for massive weights. In detail, similar to the findings of Sun et al. (2024), the top- k zeroing attack proves to be highly effective in disrupting the Llama-3 family, even for extremely large-scale models (e.g., 70B and 405B). On the other hand, the top- k retaining attack does not cause complete damage. In conclusion, these findings reveal that massive weights are predominantly learned during pre-training, highlighting their essential contribution to the overall performance of LLMs.

²<https://github.com/EleutherAI/lm-evaluation-harness>

³We use 8xA100-80G GPUs for our work; therefore, we employ an 8-bit model.

Figure 4: Mean zero-shot accuracy of top- k zeroing and retaining across various LLMs.Figure 5: Probability of experts of Mistral-8x7b for the *bos* token. In the layer with massive weights (i.e., layer 2), the router probability between experts becomes completely skewed to one expert.

Moreover, massive weights also exist in instruction-tuned LLMs such as Llama-3-8B-Instruct. These attacks are effective, as depicted in Figure 1(b). When massive weights are set to zero (i.e., darker orange box), the model repeats the same text as the user prompt. On the other hand, when all weights are set to zero except for massive weights (i.e., lighter orange box), the model retains its ability to generate text, although the generated text differs from the original.

k , which affects performance, depends on the model architecture. We examine the robustness of various LLMs against the top- k zeroing and retaining attacks, with a focus on the impact of the parameter k . Llama-2 (Touvron et al., 2023), Llama-3 (Dubey et al., 2024), Mistral (Jiang et al., 2023) and Mistral (Jiang et al., 2024), Phi-3 (Abdin et al., 2024), and Gemma-2 (Team et al., 2024) families are used. Figure 4 illustrates the mean zero-shot accuracy of LLMs under the two attacks, according to the k . In top- k zeroing, more weights are set to zero as k increases, whereas in top- k retaining, more weights are set to zero as k decreases. When k is 0 in top- k zeroing, it corresponds to the original performance without any attack, whereas, when k is 0 in top- k retaining, it sets the entire weights of \mathbf{W}_{up} and \mathbf{W}_{gate} in layer l to zero.

The Llama families are highly sensitive to massive weights. In the top- k zeroing, a noticeable performance drop occurs even when k is as small as 3, irrespective of the model’s scale. In top- k retaining, when k is set to 1 (i.e., with only one row active in \mathbf{W}_{up} and \mathbf{W}_{gate} in layer l), the performance nearly reaches the original level in smaller-scaled models ($\leq 13\text{B}$). While, for larger-scaled models ($\geq 70\text{B}$), the top-30 massive weights are required to maintain performance.

Similarly, Mistral is also disrupted, when k is set to 5. Mistral is a sparse Mixture of Experts (MoE) architecture that uses a top-2 routing mechanism, where two experts are activated among eight FFN modules in each layer. To attack the Mistral model, we identify the active experts in the layer with massive weights using the *bos* token. Figure 5 describes the probability distribution of experts in the Mistral model across all layers. Notably, it is observed that when massive activations occur, a single expert (i.e., expert 4) is assigned a significantly higher probability than the others. Therefore, we target only the \mathbf{W}_{up} and \mathbf{W}_{gate} of this expert, rather than all experts. Although Mistral does not completely break down, there is a considerable decline in performance when the top-50 massive weights are zeroed out. These results indicate that, despite the immense resources required to build high-performance LLMs, they can collapse like a house of cards even under minimal attacks.

The Phi-3 family exhibits different robustness against attacks depending on the model size. As noted by Abdin et al. (2024), the phi-3-mini (3.8B) is trained on 3.3T tokens, while the phi-3-medium (14B) is trained on 4.8T tokens. A key architectural difference from the Llama family is the use of dropout to the outputs of both the ATTN and FFN modules, formed by Eq. (2). While a specific recipe for dropout is not provided in the technical report (Abdin et al., 2024), in the case of phi-3-medium, applying dropout with longer pre-training might ensure that the residual connections contribute meaningfully, mitigating the risk of excessive dependence on massive weights.

$$h_l = \hat{h}_l + \text{dropout}(\text{FFN}(\text{LN}(\hat{h}_l))), \text{ where } \hat{h}_l = h_{l-1} + \text{dropout}(\text{ATTN}(\text{LN}(h_{l-1}))) \quad (2)$$

The Gemma-2 family is exceptionally resilient to the top- k zeroing attack, maintaining almost no loss in performance even when k is large. Additionally, even if W_{up} and W_{gate} are entirely eliminated (i.e., $k = 0$ in top- k retaining), there is no noticeable performance degradation. This family incorporates two additional LN layers after both the ATTN and FFN modules, formed by Eq. (3). These added normalization layers result in completely different hidden and intermediate states compared to other models, as described in Appendix C. Furthermore, attention sinks at the initial token are not observed in the Gemma-2 family (Appendix D).

$$h_l = \hat{h}_l + \text{LN}(\text{FFN}(\text{LN}(\hat{h}_l))), \text{ where } \hat{h}_l = h_{l-1} + \text{LN}(\text{ATTN}(\text{LN}(h_{l-1}))) \quad (3)$$

Nevertheless, because most existing open-source models, except for a few, are still heavily dependent on massive weights, it is critical to take them into account.

3 MASSIVE WEIGHTS CURRICULUM DROPOUT

In this section, we propose a straightforward plug-and-play method, termed **massive weights curriculum dropout** (`MacDrop`), during parameter-efficient fine-tuning such as low rank adaptation (Hu et al., 2022). This method applies dropout to the pre-trained massive weights with a curriculum that gradually reduces the dropout probability. The reason for applying dropout to weights (Wan et al., 2013) instead of activations (Srivastava et al., 2014) is that the number of massive activations is only k , but that of massive weights is $k \times d$, where d is the dimension of the hidden states. Note that our method is not applied to the trainable parameters of adapters. Therefore, `MacDrop` can be applied orthogonally to the process of training the adapter. Algorithm 1 describes `MacDrop` in a pseudo PyTorch (Paszke et al., 2019) style, and is implemented within the trainer code of `transformers`⁴. Initially, massive weights are identified using the *bos* token before fine-tuning (Lines 1-3). Subsequently, an adapter is trained while the pre-trained massive weights are dropped. Meanwhile, a curriculum strategy is applied to progressively enable the use of the original pre-trained weights without masking. Note that in Line 8, ‘model’ includes both the masked pre-trained network and a trainable adapter.

`MacDrop` is motivated by the observation that massive weights are predominantly learned during the pre-training phase, and that zeroing them can severely undermine LLMs. Therefore, at the early stages of fine-tuning, the objective is to reduce the reliance on massive weights, as their excessive dominance may lead the model to over-rely on specific patterns. Moreover, considering that the undamaged pre-trained model is used after fine-tuning is finished, we develop a strategy to adjust the dropout rate using a curriculum.

Algorithm 1: Top- k Massive Weights Curriculum Dropout in pseudo PyTorch style

```
// Dropout is only executed in layer  $l$ ,
// where the massive intermediate state  $h_l^{inter}$  appears.
Input:  $k$ , massive intermediate state  $h_l^{inter}$  of the bos token, initial dropout probability  $p_0$ , total steps  $T$ 

// massive activations in the intermediate state
1  $\_, \text{sorted\_indices} = \text{torch.sort}(\text{torch.abs}(h_l^{inter}), \text{descending}=\text{True})$ 
2  $\text{massive\_indices} = \text{sorted\_indices}[:k]$ 
   // massive weights
3  $\text{massive\_W\_up} = \text{copy}(\text{W\_up}[\text{massive\_indices}, :]); \text{massive\_W\_gate} = \text{copy}(\text{W\_gate}[\text{massive\_indices}, :])$ 
4 for  $t = 1$  to  $T$  do
   // decreasing dropout probability
5    $p = p_0 \times (1 - \frac{t}{T})$ 
   // pre-trained massive weights dropout
6    $\text{mask} = (\text{torch.rand}(\text{massive\_W\_up.shape}) > p).\text{int}()$ 
7    $\text{W\_up}[\text{massive\_indices}, :] *= \text{mask}; \text{W\_gate}[\text{massive\_indices}, :] *= \text{mask}$ 
8    $\text{tr\_loss\_step} = \text{training\_step}(\text{model}, \text{inputs})$ 
   // pre-trained massive weights rollback
9    $\text{W\_up}[\text{massive\_indices}, :] = \text{massive\_W\_up}; \text{W\_gate}[\text{massive\_indices}, :] = \text{massive\_W\_gate}$ 
```

⁴<https://github.com/huggingface/transformers/tree/main/src/transformers>

Table 2: Zero-shot downstream tasks performance.

Model	Method	ARC-Easy	ARC-Challenge	BoolQ	PIQA	WinoGrande	Avg.
Llama-3-8B	LoRA	79.6	58.2	83.9	82.4	75.9	76.0
	+ MacDrop	82.9	58.3	83.9	82.6	75.0	76.5
	DoRA	80.8	57.7	83.9	82.5	75.8	76.1
	+ MacDrop	81.9	58.2	83.9	82.2	75.6	76.4
Mistral-7B	LoRA	78.5	54.9	84.9	82.9	75.3	75.3
	+ MacDrop	80.9	56.7	85.0	83.0	75.3	76.2
	DoRA	78.4	55.1	85.0	82.9	75.1	75.3
	+ MacDrop	80.6	56.7	85.3	82.9	75.1	76.1

Table 3: Generation tasks performance measured by Prometheus-2-7B.

Model	Method	MT-1	MT-2	translation	summarization	QA	math reasoning	RAG	Avg.
Llama-3-8B	LoRA	3.71	3.54	4.50	3.24	4.35	3.64	3.74	3.82
	+ MacDrop	3.76	3.49	4.51	3.39	4.29	3.50	3.71	3.81
	DoRA	3.85	3.71	4.56	3.34	4.35	3.59	3.73	3.80
	+ MacDrop	3.79	3.41	4.55	3.26	4.29	3.79	3.85	3.85
Mistral-7B	LoRA	3.55	3.30	4.61	3.33	4.41	3.45	4.05	3.81
	+ MacDrop	3.75	3.42	4.58	3.26	4.35	3.30	3.98	3.81
	DoRA	3.55	3.29	4.64	3.34	4.49	3.35	3.88	3.79
	+ MacDrop	3.49	3.29	4.59	3.52	4.41	3.33	3.95	3.80

4 EXPERIMENTS

4.1 ZERO-SHOT DOWNSTREAM TASK

We fine-tune the Llama-3-8B and Mistral-7B using the alpaca_gpt4.en dataset (Peng et al., 2023) for 3 epochs (579 steps), and evaluate on five zero-shot tasks. We use two parameter-efficient fine-tuning methods, LoRA (Hu et al., 2022) and DoRA (yang Liu et al., 2024). DoRA decomposes the pre-trained weights into two components, magnitude and direction, and applies LoRA to the direction component. Our method is based on the implementation of Llama-Factory (Zheng et al., 2024)⁵. For MacDrop, k and p_0 are set to 5 and 0.8, respectively. Details for implementations are explained in Appendix A. Table 2 presents the results on zero-shot downstream tasks. For both the models and methods, MacDrop consistently leads to performance gains, especially in ARC-Easy and ARC-Challenge tasks.

4.2 GENERATION TASK

We evaluate on the generated texts of the same models in Section 4.1 using the Spec-Bench dataset (Xia et al., 2024). This benchmark includes six subtasks, each containing 80 instances: multi-turn (MT) conversation from MT-bench (Zheng et al., 2023), translation from WMT14 DE-EN (Bojar et al., 2014), summarization from CNN/Daily Mail (Nallapati et al., 2016), question answering (QA) from Natural Questions (Kwiatkowski et al., 2019), mathematical reasoning from GSM8K (Cobbe et al., 2021), and retrieval-augmented generation (RAG) from Natural Questions (Kwiatkowski et al., 2019). We utilize the direct assessment of Prometheus-2-7B (Kim et al., 2024) to evaluate the generated texts using a 5-point Likert scale. Prometheus-2-7B is an open-source language model specifically designed for evaluation purposes⁶. Table 3 presents the results on generation tasks. MT-1 and MT-2 indicate the first turn and second turn, respectively. Unfortunately, MacDrop shows limited performance improvements in generation tasks. Examples of the generated texts and judgements are provided in Appendix E.

⁵<https://github.com/hiyouga/LLaMA-Factory>

⁶<https://github.com/prometheus-eval/prometheus-eval>

4.3 ABLATION STUDY

We further provide ablation studies related to `MacDrop` using Llama-3-8B. Unless otherwise stated, for `MacDrop`, k and p_0 are set to 5 and 0.8.

4.3.1 DROPOUT SCOPE AND PROBABILITY

We investigate the effect of dropout scope and probability compared to the original performance achieved through LoRA without dropout. This ablation study is also conducted on the W_{up} and W_{gate} projection matrices in layer l . The dropout scope is divided into three categories: all weights, massive weights, all weights except for massive weights. Additionally, to assess the impact of dropout probability, it is kept constant throughout the fine-tuning process, without using a curriculum.

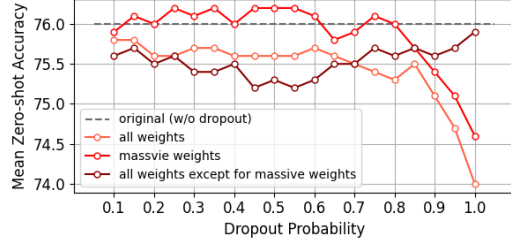


Figure 6: Mean zero-shot accuracy according to the dropout scope and probability p .

Figure 6 illustrates the mean zero-shot accuracy according to the dropout scope and dropout probability p . It is observed that among three scopes, the original performance (i.e., without dropout), represented by the dotted line at 76.0, can be surpassed only when dropout is applied solely to massive weights. Nevertheless, if strong dropout (e.g., $p \geq 0.85$) is maintained on the pre-trained massive weights during fine-tuning, performance deteriorates. This highlights the need to safeguard the pre-trained massive weights during the final stages of fine-tuning, because we are ultimately using them without causing any damage.

4.3.2 CURRICULUM METHODS AND INITIAL DROPOUT PROBABILITY

We investigate the effect of curriculum methods and initial dropout probability p_0 in `MacDrop`, when LoRA is applied. We compare four curriculum methods: step-wise linear (Step), before epoch-wise linear (Epoch(before)), after epoch-wise linear (Epoch(after)), and exponential (Exp.). In formula, Step is defined as $p = p_0 \times (1 - \frac{t_{step}}{T_{step}})$. Epoch(before) and Epoch(after) are defined as $p = p_0 \times (1 - \frac{t_{epoch} - 1}{T_{epoch}})$ and $p = p_0 \times (1 - \frac{t_{epoch}}{T_{epoch}})$, respectively.

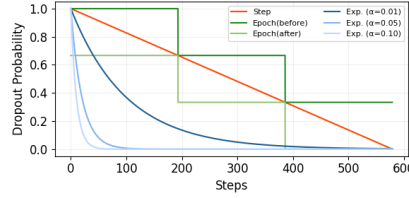


Figure 7: Curriculum methods.

Exp. is defined as $p = p_0 \times \exp(-\alpha t_{step})$. Figure 7 describes dropout probability p according to curriculum methods, when p_0 is 1.0. The distinct difference between Epoch(before) and Epoch(after) is that at the final epoch, the former continues to apply dropout to the pre-trained massive weights with a probability of $p_0 \times \frac{1}{T_{epoch}}$, while the latter fully utilizes the pre-trained massive weights.

Table 4 presents mean zero-shot accuracy according to curriculum methods and initial dropout probability p_0 . It is observed that step-based curriculum methods (e.g., Step and Exp.) generally achieve greater performance improvements compared to epoch-based curriculum methods (e.g., Epoch(before) and Epoch(after)). Nevertheless, when the initial dropout probability is relatively low (e.g., $p_0 \leq 0.2$), even step-based curriculum methods fail to bring any performance gain compared to the original performance of 76.0. Additionally, it is shown that using a smaller α in the Exp. method leads to greater performance improvements, suggesting that a rapid decline in dropout probability to zero can diminish the effectiveness of `MacDrop`. On the other hand, for the Step and Epoch(before) methods, a significant performance drop is observed at a p_0 value of 1.0, highlighting the necessity of a near-zero dropout probability for the end of fine-tuning. In conclusion, for `MacDrop`, we recommend using the Step or Exp. with a smaller α , initiated from a moderately high p_0 .

Table 4: Mean zero-shot accuracy according to curriculum methods and initial dropout probability.

Curriculum Method	p_0			
	0.2	0.5	0.8	1.0
Step	76.0	76.3	76.5	75.5
Epoch(before)	76.1	76.1	76.1	75.5
Epoch(after)	75.9	76.0	76.2	76.3
Exp. ($\alpha = 0.01$)	76.0	76.2	76.5	76.4
Exp. ($\alpha = 0.05$)	76.0	76.1	76.2	76.3
Exp. ($\alpha = 0.10$)	76.0	76.1	76.1	76.2
Mean	76.0	76.1	76.3	76.0

5 RELATED WORK

The attention sinks phenomenon and their importance, uncovered by Xiao et al. (2024), have been widely used to compress key-value caches. For quantization, KVQuant (Hooper et al., 2024) applies attention sink-aware quantization, which retains only the first token in fp16. CushionCache (Son et al., 2024) inserts sink tokens into the prefix to mitigate massive activations in the middle of the sequence, enhancing the performance of quantized models. For token eviction and token merging, sink tokens are never evicted or merged; they remain unchanged (Xiao et al., 2024; Ge et al., 2024; Li et al., 2024; Zhang et al., 2023; Wang et al., 2024; Zhang et al., 2024).

Nevertheless, there has been limited in-depth research on the phenomenon itself. In fact, the idea of global attentions, such as [CLS] and [SEP] tokens—similar to attention sinks—was introduced and emphasized even before the LLM era (Zaheer et al., 2020; Beltagy et al., 2020). In the LLM era, Yu et al. (2024) showed that sink tokens can appear not only at the beginning of a sentence but also in the middle, and they are often shown to be nonsemantic (e.g., ‘.’). Sun et al. (2024) discovered the presence of massive activations in the hidden state space of sink tokens, demonstrating that massive activations trigger the attention sinks phenomenon. Meanwhile, in vision transformers, similar phenomenon is observed (Darcet et al., 2024). They showed that training with register tokens, which is additional meaningless tokens similar to sink tokens, resulted in improved dense prediction and interpretability. Different from previous work, we explore this phenomenon in the weight space.

6 CONCLUSION

In this paper, we explore the weight space of LLMs and identify the presence of massive weights within a FFN module in an early layer, which are predominantly pre-trained and have a significant impact on the performance of LLMs. Based on our observation, we propose a plug-and-play fine-tuning method called `MacDrop`, which applies dropout to the pre-trained massive weights, rather than to the parameters of adapters, during parameter-efficient fine-tuning. We hope that our findings will inspire future research in weight space of LLMs, including model merging (Li et al., 2023) and model editing (Yao et al., 2023).

REPRODUCIBILITY

For our analysis in Section 2, we conduct a consistent and reproducible analysis using only the *bos* token (Section 2.2) and provide the specific position of massive weights across various models in Appendix B. For our algorithm, `MacDrop`, we provide PyTorch-style pseudo code in Section 3 and training details in Appendix A. Furthermore, we present github links for all our implementations with footnotes, when necessary.

REFERENCES

- Marah Abdin, Sam Ade Jacobs, Ammar Ahmad Awan, Jyoti Aneja, Ahmed Awadallah, Hany Awadalla, Nguyen Bach, Amit Bahree, Arash Bakhtiari, Harkirat Behl, et al. Phi-3 technical report: A highly capable language model locally on your phone. *arXiv preprint arXiv:2404.14219*, 2024.
- Josh Achiam, Steven Adler, Sandhini Agarwal, Lama Ahmad, Ilge Akkaya, Florencia Leoni Aleman, Diogo Almeida, Janko Altenschmidt, Sam Altman, Shyamal Anadkat, et al. Gpt-4 technical report. *arXiv preprint arXiv:2303.08774*, 2023.
- Jimmy Lei Ba. Layer normalization. *arXiv preprint arXiv:1607.06450*, 2016.
- Iz Beltagy, Matthew E. Peters, and Arman Cohan. Longformer: The long-document transformer. *arXiv:2004.05150*, 2020.
- Yonatan Bisk, Rowan Zellers, Jianfeng Gao, Yejin Choi, et al. Piqa: Reasoning about physical commonsense in natural language. In *Proceedings of the AAAI conference on artificial intelligence*, volume 34, pp. 7432–7439, 2020.

- Ondřej Bojar, Christian Buck, Christian Federmann, Barry Haddow, Philipp Koehn, Johannes Lebeling, Christof Monz, Pavel Pecina, Matt Post, Herve Saint-Amand, Radu Soricut, Lucia Specia, and Aleš Tamchyna. Findings of the 2014 workshop on statistical machine translation. In Ondřej Bojar, Christian Buck, Christian Federmann, Barry Haddow, Philipp Koehn, Christof Monz, Matt Post, and Lucia Specia (eds.), *Proceedings of the Ninth Workshop on Statistical Machine Translation*, pp. 12–58, Baltimore, Maryland, USA, June 2014. Association for Computational Linguistics. doi: 10.3115/v1/W14-3302. URL <https://aclanthology.org/W14-3302>.
- Christopher Clark, Kenton Lee, Ming-Wei Chang, Tom Kwiatkowski, Michael Collins, and Kristina Toutanova. BoolQ: Exploring the surprising difficulty of natural yes/no questions. In Jill Burstein, Christy Doran, and Thamar Solorio (eds.), *Proceedings of the 2019 Conference of the North American Chapter of the Association for Computational Linguistics: Human Language Technologies, Volume 1 (Long and Short Papers)*, pp. 2924–2936, Minneapolis, Minnesota, June 2019. Association for Computational Linguistics. doi: 10.18653/v1/N19-1300. URL <https://aclanthology.org/N19-1300>.
- Peter Clark, Isaac Cowhey, Oren Etzioni, Tushar Khot, Ashish Sabharwal, Carissa Schoenick, and Oyvind Tafjord. Think you have solved question answering? try arc, the ai2 reasoning challenge. *arXiv preprint arXiv:1803.05457*, 2018.
- Karl Cobbe, Vineet Kosaraju, Mohammad Bavarian, Mark Chen, Heewoo Jun, Lukasz Kaiser, Matthias Plappert, Jerry Tworek, Jacob Hilton, Reiichiro Nakano, et al. Training verifiers to solve math word problems. *arXiv preprint arXiv:2110.14168*, 2021.
- Timothée Darcet, Maxime Oquab, Julien Mairal, and Piotr Bojanowski. Vision transformers need registers. In *The Twelfth International Conference on Learning Representations*, 2024. URL <https://openreview.net/forum?id=2dnO3LLiJl>.
- Abhimanyu Dubey, Abhinav Jauhri, Abhinav Pandey, Abhishek Kadian, Ahmad Al-Dahle, Aiesha Letman, Akhil Mathur, Alan Schelten, Amy Yang, Angela Fan, et al. The llama 3 herd of models. *arXiv preprint arXiv:2407.21783*, 2024.
- Suyu Ge, Yunan Zhang, Liyuan Liu, Minjia Zhang, Jiawei Han, and Jianfeng Gao. Model tells you what to discard: Adaptive KV cache compression for LLMs. In *The Twelfth International Conference on Learning Representations*, 2024. URL <https://openreview.net/forum?id=uNrFpDPMYo>.
- Kaiming He, Xiangyu Zhang, Shaoqing Ren, and Jian Sun. Deep residual learning for image recognition. In *Proceedings of the IEEE conference on computer vision and pattern recognition*, pp. 770–778, 2016.
- Coleman Hooper, Sehoon Kim, Hiva Mohammadzadeh, Michael W Mahoney, Yakun Sophia Shao, Kurt Keutzer, and Amir Gholami. Kvquant: Towards 10 million context length llm inference with kv cache quantization. *arXiv preprint arXiv:2401.18079*, 2024.
- Edward J Hu, yelong shen, Phillip Wallis, Zeyuan Allen-Zhu, Yanzhi Li, Shean Wang, Lu Wang, and Weizhu Chen. LoRA: Low-rank adaptation of large language models. In *International Conference on Learning Representations*, 2022. URL <https://openreview.net/forum?id=nZeVKeeFYf9>.
- Albert Q Jiang, Alexandre Sablayrolles, Arthur Mensch, Chris Bamford, Devendra Singh Chaplot, Diego de las Casas, Florian Bressand, Gianna Lengyel, Guillaume Lample, Lucile Saulnier, et al. Mistral 7b. *arXiv preprint arXiv:2310.06825*, 2023.
- Albert Q Jiang, Alexandre Sablayrolles, Antoine Roux, Arthur Mensch, Blanche Savary, Chris Bamford, Devendra Singh Chaplot, Diego de las Casas, Emma Bou Hanna, Florian Bressand, et al. Mixtral of experts. *arXiv preprint arXiv:2401.04088*, 2024.
- Seungone Kim, Juyoung Suk, Shayne Longpre, Bill Yuchen Lin, Jamin Shin, Sean Welleck, Graham Neubig, Moontae Lee, Kyungjae Lee, and Minjoon Seo. Prometheus 2: An open source language model specialized in evaluating other language models. *arXiv preprint arXiv:2405.01535*, 2024.

- Tom Kwiatkowski, Jennimaria Palomaki, Olivia Redfield, Michael Collins, Ankur Parikh, Chris Alberti, Danielle Epstein, Illia Polosukhin, Jacob Devlin, Kenton Lee, Kristina Toutanova, Llion Jones, Matthew Kelcey, Ming-Wei Chang, Andrew M. Dai, Jakob Uszkoreit, Quoc Le, and Slav Petrov. Natural questions: A benchmark for question answering research. *Transactions of the Association for Computational Linguistics*, 7:452–466, 2019. doi: 10.1162/tacl.a.00276. URL <https://aclanthology.org/Q19-1026>.
- Yanis Labrak, Adrien Bazoge, Emmanuel Morin, Pierre-Antoine Gourraud, Mickael Rouvier, and Richard Dufour. BioMistral: A collection of open-source pretrained large language models for medical domains. In Lun-Wei Ku, Andre Martins, and Vivek Srikumar (eds.), *Findings of the Association for Computational Linguistics ACL 2024*, pp. 5848–5864, Bangkok, Thailand and virtual meeting, August 2024. Association for Computational Linguistics. URL <https://aclanthology.org/2024.findings-acl.348>.
- Weishi Li, Yong Peng, Miao Zhang, Liang Ding, Han Hu, and Li Shen. Deep model fusion: A survey. *arXiv preprint arXiv:2309.15698*, 2023.
- Yuhong Li, Yingbing Huang, Bowen Yang, Bharat Venkitesh, Acyr Locatelli, Hanchen Ye, Tianle Cai, Patrick Lewis, and Deming Chen. Snapkv: Llm knows what you are looking for before generation. *arXiv preprint arXiv:2404.14469*, 2024.
- Shayne Longpre, Gregory Yauney, Emily Reif, Katherine Lee, Adam Roberts, Barret Zoph, Denny Zhou, Jason Wei, Kevin Robinson, David Mimno, and Daphne Ippolito. A pretrainer’s guide to training data: Measuring the effects of data age, domain coverage, quality, & toxicity. In Kevin Duh, Helena Gomez, and Steven Bethard (eds.), *Proceedings of the 2024 Conference of the North American Chapter of the Association for Computational Linguistics: Human Language Technologies (Volume 1: Long Papers)*, pp. 3245–3276, Mexico City, Mexico, June 2024. Association for Computational Linguistics. doi: 10.18653/v1/2024.naacl-long.179. URL <https://aclanthology.org/2024.naacl-long.179>.
- Stephen Merity, Caiming Xiong, James Bradbury, and Richard Socher. Pointer sentinel mixture models. In *International Conference on Learning Representations*, 2017. URL <https://openreview.net/forum?id=Byj72udxe>.
- Arindam Mitra, Hamed Khanpour, Corby Rosset, and Ahmed Awadallah. Orca-math: Unlocking the potential of slms in grade school math. *arXiv preprint arXiv:2402.14830*, 2024.
- Ramesh Nallapati, Bowen Zhou, Cicero dos Santos, Çağlar Gulçehre, and Bing Xiang. Abstractive text summarization using sequence-to-sequence RNNs and beyond. In Stefan Riezler and Yoav Goldberg (eds.), *Proceedings of the 20th SIGNLL Conference on Computational Natural Language Learning*, pp. 280–290, Berlin, Germany, August 2016. Association for Computational Linguistics. doi: 10.18653/v1/K16-1028. URL <https://aclanthology.org/K16-1028>.
- Adam Paszke, Sam Gross, Francisco Massa, Adam Lerer, James Bradbury, Gregory Chanan, Trevor Killeen, Zeming Lin, Natalia Gimelshein, Luca Antiga, Alban Desmaison, Andreas Kopf, Edward Yang, Zachary DeVito, Martin Raison, Alykhan Tejani, Sasank Chilamkurthy, Benoit Steiner, Lu Fang, Junjie Bai, and Soumith Chintala. Pytorch: An imperative style, high-performance deep learning library. In H. Wallach, H. Larochelle, A. Beygelzimer, F. d’Alché-Buc, E. Fox, and R. Garnett (eds.), *Advances in Neural Information Processing Systems*, volume 32. Curran Associates, Inc., 2019. URL https://proceedings.neurips.cc/paper_files/paper/2019/file/bdbca288fee7f92f2bfa9f7012727740-Paper.pdf.
- Baolin Peng, Chunyuan Li, Pengcheng He, Michel Galley, and Jianfeng Gao. Instruction tuning with gpt-4. *arXiv preprint arXiv:2304.03277*, 2023.
- Jack W. Rae, Anna Potapenko, Siddhant M. Jayakumar, Chloe Hillier, and Timothy P. Lillcrap. Compressive transformers for long-range sequence modelling. In *International Conference on Learning Representations*, 2020. URL <https://openreview.net/forum?id=SylKikSYDH>.

- Colin Raffel, Noam Shazeer, Adam Roberts, Katherine Lee, Sharan Narang, Michael Matena, Yanqi Zhou, Wei Li, and Peter J Liu. Exploring the limits of transfer learning with a unified text-to-text transformer. *Journal of machine learning research*, 21(140):1–67, 2020.
- Baptiste Roziere, Jonas Gehring, Fabian Gloeckle, Sten Sootla, Itai Gat, Xiaoqing Ellen Tan, Yossi Adi, Jingyu Liu, Romain Sauvestre, Tal Remez, et al. Code llama: Open foundation models for code. *arXiv preprint arXiv:2308.12950*, 2023.
- Keisuke Sakaguchi, Ronan Le Bras, Chandra Bhagavatula, and Yejin Choi. Winogrande: An adversarial winograd schema challenge at scale. *Communications of the ACM*, 64(9):99–106, 2021.
- Zhiqiang Shen, Tianhua Tao, Liqun Ma, Willie Neiswanger, Zhengzhong Liu, Hongyi Wang, Bowen Tan, Joel Hestness, Natalia Vassilieva, Daria Soboleva, et al. Slimpajama-dc: Understanding data combinations for llm training. *arXiv preprint arXiv:2309.10818*, 2023.
- Seungwoo Son, Wonpyo Park, Woohyun Han, Kyuyeun Kim, and Jaeho Lee. Prefixing attention sinks can mitigate activation outliers for large language model quantization. *arXiv preprint arXiv:2406.12016*, 2024.
- Nitish Srivastava, Geoffrey Hinton, Alex Krizhevsky, Ilya Sutskever, and Ruslan Salakhutdinov. Dropout: a simple way to prevent neural networks from overfitting. *The journal of machine learning research*, 15(1):1929–1958, 2014.
- Mingjie Sun, Xinlei Chen, J Zico Kolter, and Zhuang Liu. Massive activations in large language models. In *First Conference on Language Modeling*, 2024. URL <https://openreview.net/forum?id=F7aAhfitX6>.
- Gemma Team, Morgane Riviere, Shreya Pathak, Pier Giuseppe Sessa, Cassidy Hardin, Surya Bhatiraju, Léonard Hussenot, Thomas Mesnard, Bobak Shahriari, Alexandre Ramé, et al. Gemma 2: Improving open language models at a practical size. *arXiv preprint arXiv:2408.00118*, 2024.
- Hugo Touvron, Louis Martin, Kevin Stone, Peter Albert, Amjad Almahairi, Yasmine Babaei, Nikolay Bashlykov, Soumya Batra, Prajjwal Bhargava, Shruti Bhosale, et al. Llama 2: Open foundation and fine-tuned chat models. *arXiv preprint arXiv:2307.09288*, 2023.
- Ashish Vaswani, Noam Shazeer, Niki Parmar, Jakob Uszkoreit, Llion Jones, Aidan N Gomez, Łukasz Kaiser, and Illia Polosukhin. Attention is all you need. In I. Guyon, U. Von Luxburg, S. Bengio, H. Wallach, R. Fergus, S. Vishwanathan, and R. Garnett (eds.), *Advances in Neural Information Processing Systems*, volume 30. Curran Associates, Inc., 2017. URL https://proceedings.neurips.cc/paper_files/paper/2017/file/3f5ee243547dee91fbd053c1c4a845aa-Paper.pdf.
- Li Wan, Matthew Zeiler, Sixin Zhang, Yann Le Cun, and Rob Fergus. Regularization of neural networks using dropconnect. In *International conference on machine learning*, pp. 1058–1066. PMLR, 2013.
- Zheng Wang, Boxiao Jin, Zhongzhi Yu, and Minjia Zhang. Model tells you where to merge: Adaptive kv cache merging for llms on long-context tasks. *arXiv preprint arXiv:2407.08454*, 2024.
- Shijie Wu, Ozan Irsoy, Steven Lu, Vadim Dabravolski, Mark Dredze, Sebastian Gehrmann, Prabhakaran Kambadur, David Rosenberg, and Gideon Mann. Bloomberggpt: A large language model for finance. *arXiv preprint arXiv:2303.17564*, 2023.
- Heming Xia, Zhe Yang, Qingxiu Dong, Peiyi Wang, Yongqi Li, Tao Ge, Tianyu Liu, Wenjie Li, and Zhifang Sui. Unlocking efficiency in large language model inference: A comprehensive survey of speculative decoding. In Lun-Wei Ku, Andre Martins, and Vivek Srikumar (eds.), *Findings of the Association for Computational Linguistics ACL 2024*, pp. 7655–7671, Bangkok, Thailand and virtual meeting, August 2024. Association for Computational Linguistics. URL <https://aclanthology.org/2024.findings-acl.456>.
- Guangxuan Xiao, Yuandong Tian, Beidi Chen, Song Han, and Mike Lewis. Efficient streaming language models with attention sinks. In *The Twelfth International Conference on Learning Representations*, 2024. URL <https://openreview.net/forum?id=NG7sS51zVF>.

- Shih yang Liu, Chien-Yi Wang, Hongxu Yin, Pavlo Molchanov, Yu-Chiang Frank Wang, Kwang-Ting Cheng, and Min-Hung Chen. DoRA: Weight-decomposed low-rank adaptation. In *Forty-first International Conference on Machine Learning*, 2024. URL <https://openreview.net/forum?id=3d5CIRG1n2>.
- Yunzhi Yao, Peng Wang, Bozhong Tian, Siyuan Cheng, Zhoubo Li, Shumin Deng, Huajun Chen, and Ningyu Zhang. Editing large language models: Problems, methods, and opportunities. In Houda Bouamor, Juan Pino, and Kalika Bali (eds.), *Proceedings of the 2023 Conference on Empirical Methods in Natural Language Processing*, pp. 10222–10240, Singapore, December 2023. Association for Computational Linguistics. doi: 10.18653/v1/2023.emnlp-main.632. URL <https://aclanthology.org/2023.emnlp-main.632>.
- Zhongzhi Yu, Zheng Wang, Yonggan Fu, Huihong Shi, Khalid Shaikh, and Yingyan Celine Lin. Unveiling and harnessing hidden attention sinks: Enhancing large language models without training through attention calibration. In Ruslan Salakhutdinov, Zico Kolter, Katherine Heller, Adrian Weller, Nuria Oliver, Jonathan Scarlett, and Felix Berkenkamp (eds.), *Proceedings of the 41st International Conference on Machine Learning*, volume 235 of *Proceedings of Machine Learning Research*, pp. 57659–57677. PMLR, 21–27 Jul 2024. URL <https://proceedings.mlr.press/v235/yu241.html>.
- Manzil Zaheer, Guru Guruganesh, Kumar Avinava Dubey, Joshua Ainslie, Chris Alberti, Santiago Ontanon, Philip Pham, Anirudh Ravula, Qifan Wang, Li Yang, et al. Big bird: Transformers for longer sequences. *Advances in neural information processing systems*, 33:17283–17297, 2020.
- Yuxin Zhang, Yuxuan Du, Gen Luo, Yunshan Zhong, Zhenyu Zhang, Shiwei Liu, and Rongrong Ji. Cam: Cache merging for memory-efficient LLMs inference. In *Forty-first International Conference on Machine Learning*, 2024. URL <https://openreview.net/forum?id=LCTmppB165>.
- Zhenyu Zhang, Ying Sheng, Tianyi Zhou, Tianlong Chen, Lianmin Zheng, Ruisi Cai, Zhao Song, Yuandong Tian, Christopher Ré, Clark Barrett, Zhangyang "Atlas" Wang, and Beidi Chen. H2o: Heavy-hitter oracle for efficient generative inference of large language models. In A. Oh, T. Naumann, A. Globerson, K. Saenko, M. Hardt, and S. Levine (eds.), *Advances in Neural Information Processing Systems*, volume 36, pp. 34661–34710. Curran Associates, Inc., 2023. URL https://proceedings.neurips.cc/paper_files/paper/2023/file/6ceefa7b15572587b78ecfceb2827f8-Paper-Conference.pdf.
- Yang Zhao, Li Du, Xiao Ding, Kai Xiong, Zhouhao Sun, Shi Jun, Ting Liu, and Bing Qin. Deciphering the impact of pretraining data on large language models through machine unlearning. In Lun-Wei Ku, Andre Martins, and Vivek Srikumar (eds.), *Findings of the Association for Computational Linguistics ACL 2024*, pp. 9386–9406, Bangkok, Thailand and virtual meeting, August 2024. Association for Computational Linguistics. URL <https://aclanthology.org/2024.findings-acl.559>.
- Lianmin Zheng, Wei-Lin Chiang, Ying Sheng, Siyuan Zhuang, Zhanghao Wu, Yonghao Zhuang, Zi Lin, Zhuohan Li, Dacheng Li, Eric Xing, Hao Zhang, Joseph E. Gonzalez, and Ion Stoica. Judging LLM-as-a-judge with MT-bench and chatbot arena. In *Thirty-seventh Conference on Neural Information Processing Systems Datasets and Benchmarks Track*, 2023. URL <https://openreview.net/forum?id=uccHPGD1ao>.
- Yaowei Zheng, Richong Zhang, Junhao Zhang, Yanhan Ye, and Zheyang Luo. Llamafactory: Unified efficient fine-tuning of 100+ language models. *arXiv preprint arXiv:2403.13372*, 2024.

A IMPLEMENTATION DETAILS

We use 8xA100-80GB, for our all implementations. As discussed in Section 2.2, we use only the *bos* token to analyze massive activations and massive weights, and design `MacDrop`. In Section 2.2, we use the example and visualization of massive activations. For parameter-efficient fine-tuning, Llama-Factory is used and configurations are summarized in Table 5. For evaluation, we use the code of massive activations for perplexity, use `lm-eval-harness` for zero-shot accuracy, and use `FastChat` and `Prometheus` for generation tasks. Related papers and codes are cited in the main.

Table 5: Configuration for low rank adaptation (LoRA and DoRA).

Argument	Setting
dataset	alpaca_gpt4_en
validation size	0.05
per device train batch size	8
gradient accumulation steps	4
learning rate	1e-4
num train epochs	3
warmup ratio	0.05
adam β_1	0.9
adam β_2	0.999
lora target	all linear layers except for embedding layer and lm head
lora rank	16
lora alpha	16

B POSITION OF MASSIVE WEIGHTS

Table 6 summarizes the position of massive weights across various models.

Table 6: Layer and indices of top-5 massive weights.

Model	Layer	Top-5 indices
Llama-2-7b-hf	2	[7890, 10411, 1192, 8731, 5843]
Llama-2-7b-chat-hf	2	[7890, 10411, 1192, 8731, 5843]
Llama-2-13b-hf	4	[7678, 8811, 11371, 6619, 12281]
Llama-2-13b-chat-hf	4	[7678, 8811, 11371, 6619, 12281]
Meta-Llama-3-8B	2	[2427, 198, 6412, 12657, 591]
Meta-Llama-3-8B-Instruct	2	[2427, 198, 6412, 591, 12657]
Meta-Llama-3-70B	4	[16581, 3590, 16039, 19670, 13266]
Meta-Llama-3-70B-Instruct	4	[16581, 3590, 16039, 19670, 13266]
Meta-Llama-3.1-405B (8bit)	6	[11891, 30740, 2392, 36238, 12328]
Meta-Llama-3.1-405B-Instruct (8bit)	6	[11891, 30740, 36238, 2392, 1073]
Mistral-7B-v0.1	2	[7310, 8572, 2514, 1878, 8693]
Mistral-7B-Instruct-v0.1	2	[7310, 8572, 2514, 2484, 1878]
Mixtral-8x7B-v0.1	2 (expert 4)	[7310, 7530, 11981, 7492, 3178]
Mixtral-8x7B-Instruct-v0.1	2 (expert 4)	[7310, 11981, 2514, 7530, 3178]
Phi-3-mini-4k-instruct	3	[808, 340, 3644, 2473, 2987]
Phi-3-medium-4k-instruct	6	[181, 7540, 19, 15874, 5137]
gemma-2-2b	-	-
gemma-2-2b-it	-	-
gemma-2-9b	-	-
gemma-2-9b-it	-	-
gemma-2-27b	-	-
gemma-2-27b-it	-	-

C FUTHER ANALYSIS FOR VARIOUS LLMs

We investigate various LLM families: Llama-2 (Touvron et al., 2023), Llama-3 (Dubey et al., 2024), Mistral (Jiang et al., 2023) and Mixtral (Jiang et al., 2024), Phi-3 (Abdin et al., 2024), and Gemma-2 (Team et al., 2024). Similar to Figure 3 in the main, we provide the top-3 and median magnitudes in the hidden states and the intermediate states throughout the layers. In subcaptions, H and I represent the hidden state and the intermediate state, respectively.

When comparing pre-trained LLMs (e.g., Llama-2-7b-hf) and instruction-tuned LLMs (e.g., Llama-2-7b-chat-hf) of the same model, the shape of their graphs is almost identical. This suggests that massive weights are formed during the pre-training process. Llama-2, Llama-3, Mistral, Mixtral, and Phi-3 exhibit similar patterns in their hidden states: following a single explosive amplification in an early layer, massive activations are sustained through residual connections almost until the final layer, although Phi-3 experiences a few additional amplifications. In fact, as we discuss in the main, such an explosion initially occurs in the intermediate state, and this phenomenon is observed across different models. However, the behavior of the Gemma-2 family significantly deviates from that of other models. Firstly, instead of the values being maintained in the hidden state, Gemma-2 shows a continuous increase followed by a decrease. Secondly, the magnitude of the explosion observed in the intermediate state is considerably lower compared to other models. These unique characteristics suggest that Gemma-2 operates under different internal dynamics, which may influence its overall performance and stability.

C.1 LLAMA-2 FAMILY

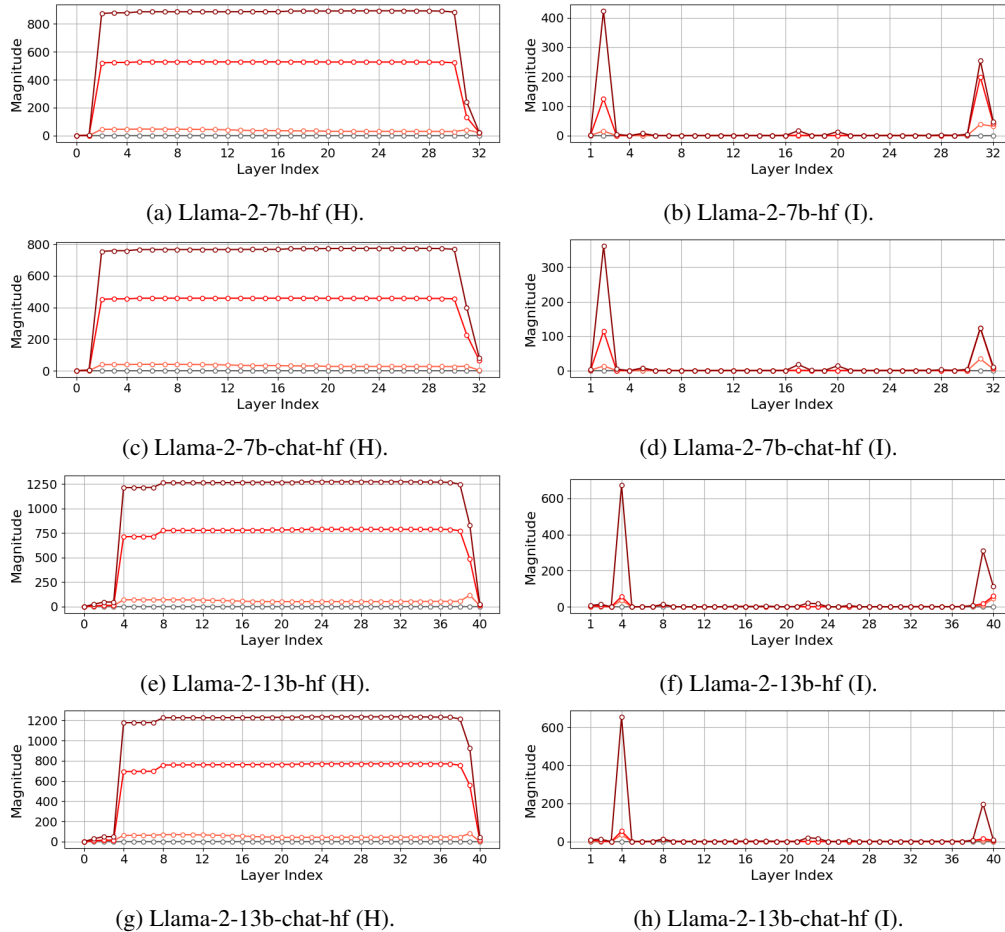


Figure 8: (Left) Hidden state and (Right) intermediate state of Llama-2 family.

C.2 LLAMA-3 FAMILY

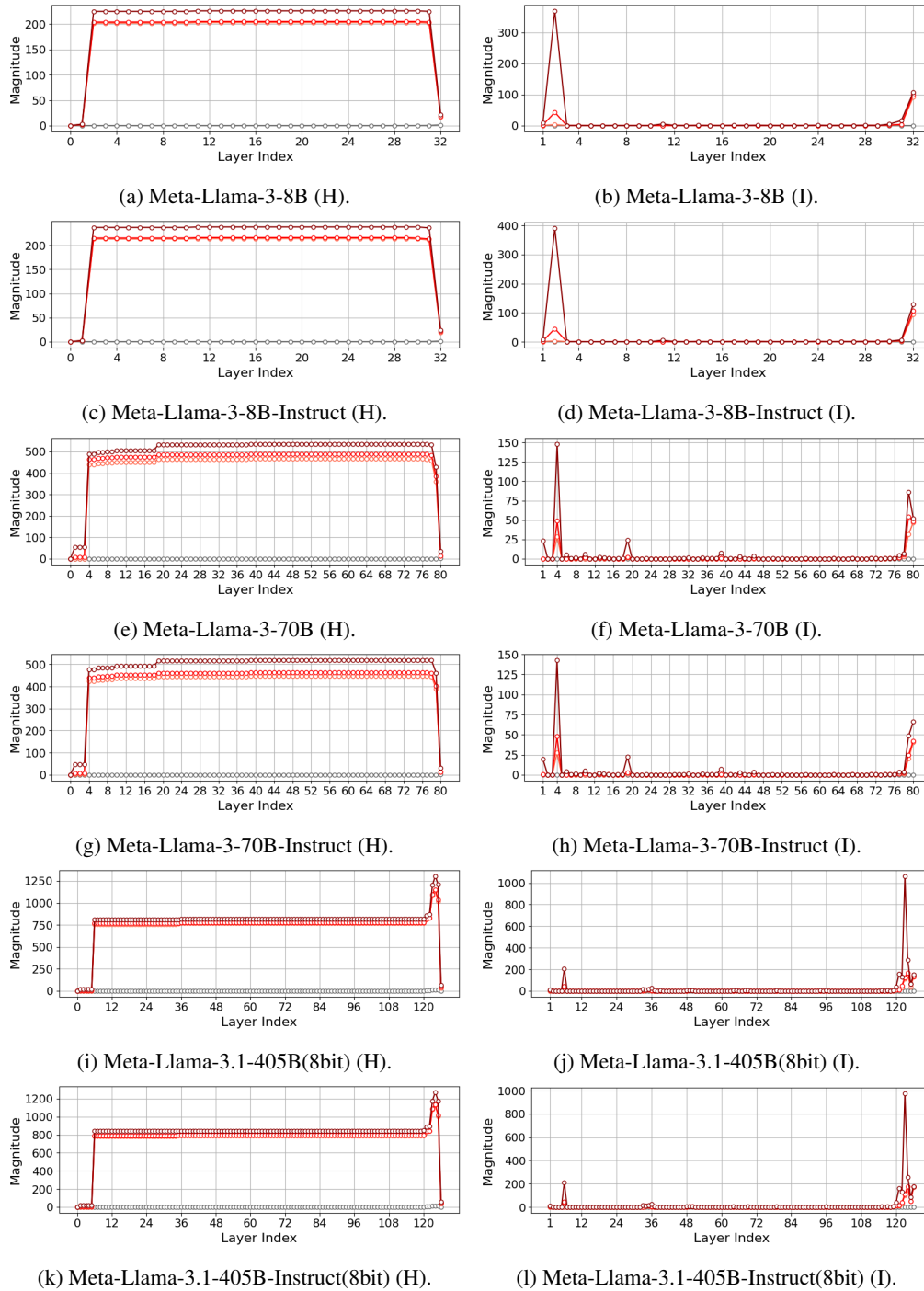


Figure 9: (Left) Hidden state and (Right) intermediate state of Llama-3/3.1 family.

C.3 MISTRAL AND MIXTRAL FAMILY

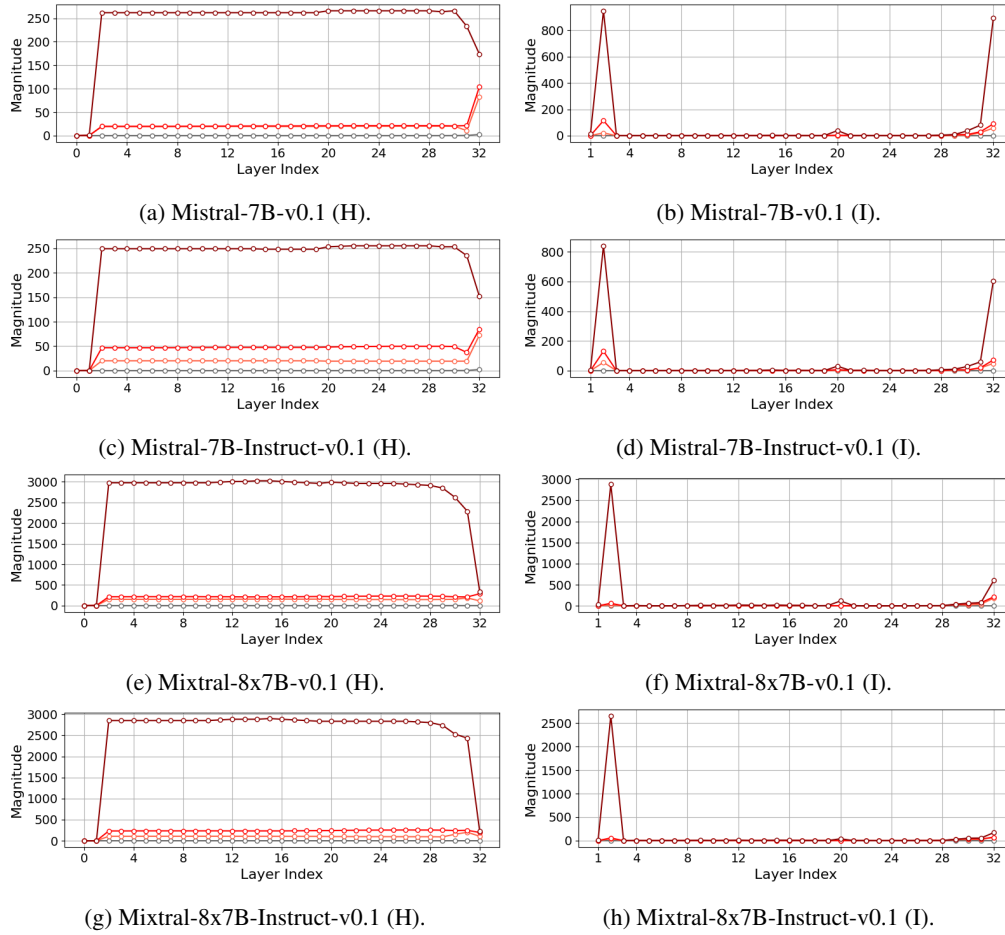


Figure 10: (Left) Hidden state and (Right) intermediate state of Mistral and Mixtral family.

C.4 PHI-3 FAMILY

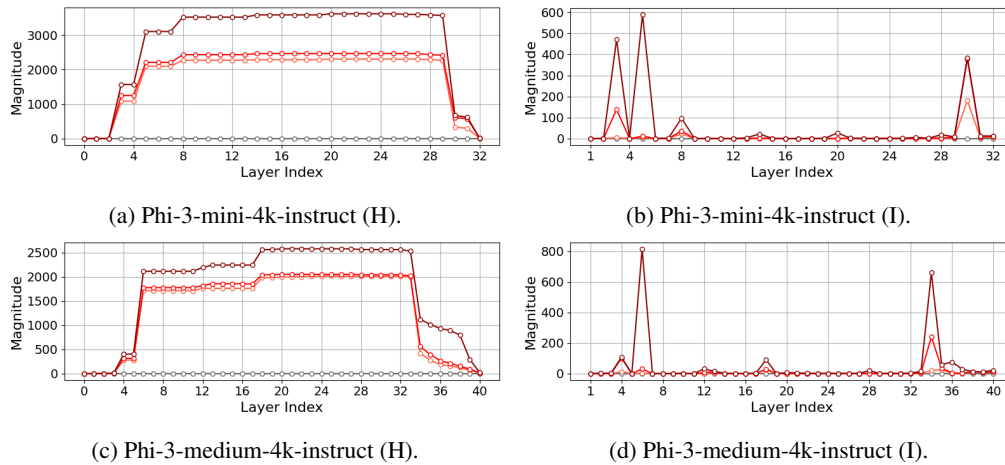


Figure 11: (Left) Hidden state and (Right) intermediate state of Phi-3 family.

C.5 GEMMA-2 FAMILY

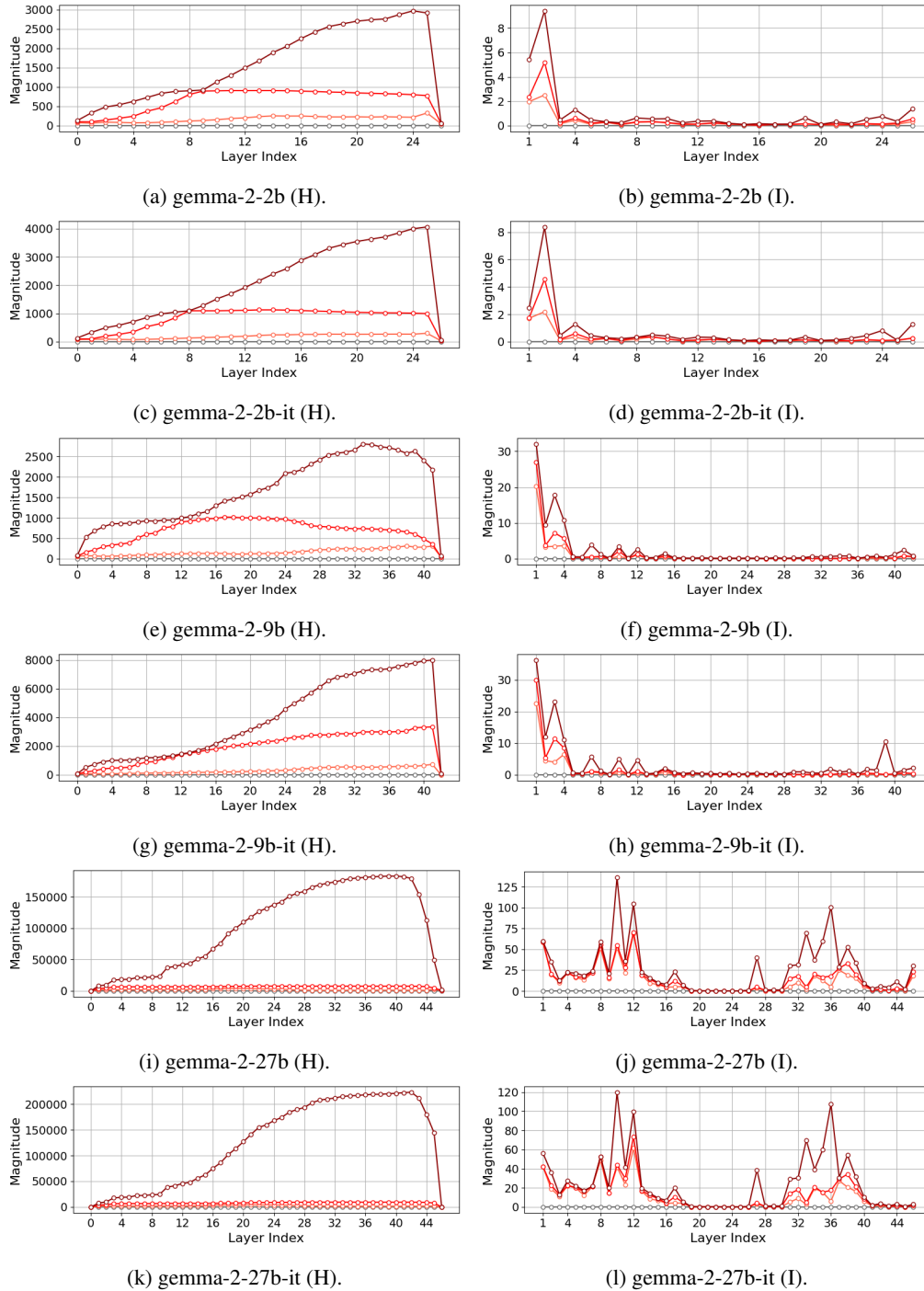
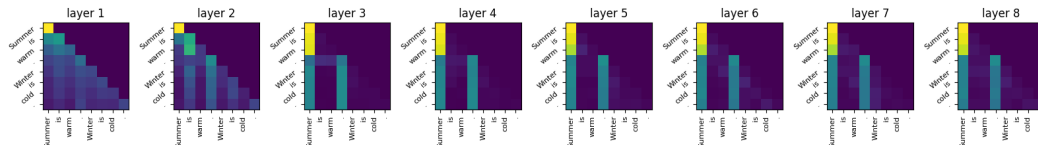


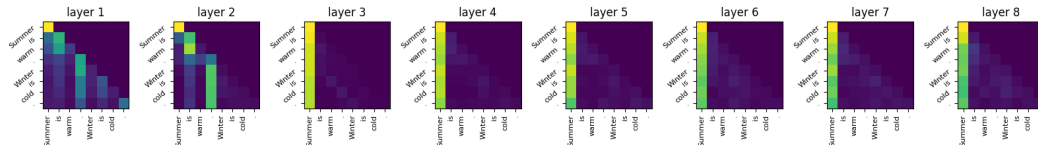
Figure 12: (Left) Hidden state and (Right) intermediate state of Gemma-2 family.

D ATTENTION SINKS

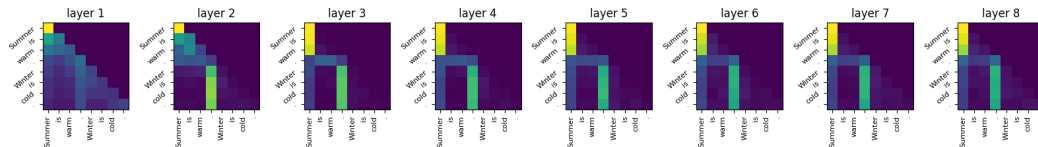
Figure 13 describes attention after Softmax in the early layers (from layer 1 to layer 8) across various models. Attention sinks are observed in the layers after the massive weights layer. In Llama-2-7B (Figure 13(a)), Mistral-7B (Figure 13(c)), and Mixtral-8x7B (Figure 13(d)), sink tokens are the initial token (‘Summer’) and the first delimiter token (‘.’), discovered by Sun et al. (2024). In Llama-3-8B (Figure 13(b)) and Phi-3-mini (Figure 13(e)), sink token is the only the initial token (‘Summer’). Interestingly, in these five models, it is commonly observed that significant attention is concentrated on non-semantic tokens (‘.’) before attention sinks occur. However, in Gemma-2 (Figure 13(f)), attention sinks do not happen and attention is primarily assigned to local tokens. Note that what we provide is the average of the heads, and there might be heads that do not fully sink when viewed individually.



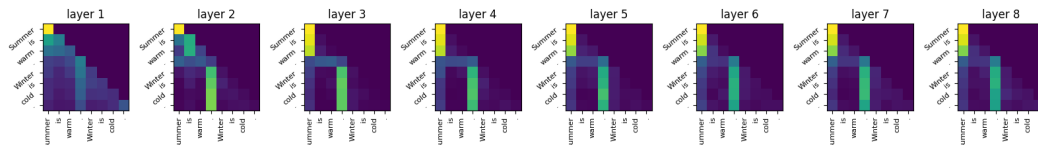
(a) Llama-2-7B. Attention sinks happen from layer 3.



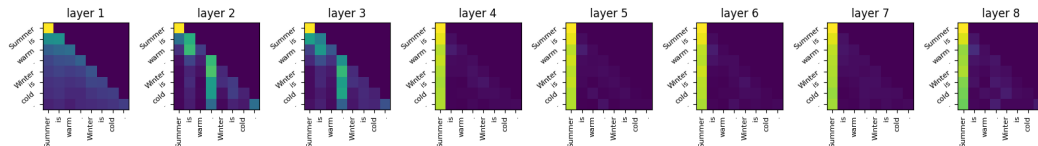
(b) Llama-3-8B. Attention sinks happen from layer 3.



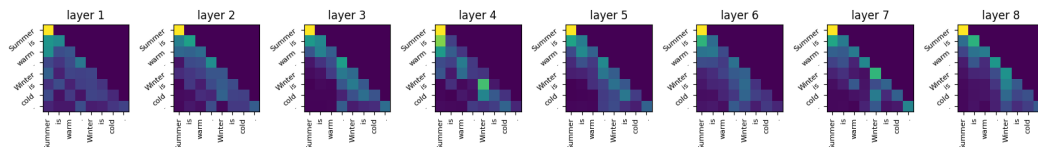
(c) Mistral-7B. Attention sinks happen from layer 3.



(d) Mixtral-8x7B. Attention sinks happen from layer 3.



(e) Phi-3-mini-4k-instruct. Attention sinks happen from layer 4.



(f) gemma-2-2b. Attention sinks do not happen.

Figure 13: Attention after Softmax.

E EXAMPLES IN GENERATION TASK

Assistant A and B indicate Llama-3-8B with and without MacDrop, respectively.

Table 7: Example of generation task (translation).

User	Translate German to English: St. Hubertus war der Sage nach ein recht rücksichtsloser Jäger, der durch eine Vision bekehrt und später zum Bischof von Lüttich ernannt wurde.
Reference answer	St. Hubert was, according to legend, a truly ruthless hunter, who converted following a vision and was later appointed Bishop of Lüttich.
Assistant A	According to legend, St. Hubertus was a rather ruthless hunter who was converted and later appointed as the Bishop of Liège after a vision.
Judgment for A	The response provided a translation that was generally accurate and relevant to the user’s request. However, there were minor inaccuracies in the phrasing, such as “rather ruthless” instead of “truly ruthless,” which slightly deviated from the original text. Additionally, the term “Liège” was used instead of “Lüttich,” which is the correct name of the city in the original German text. Despite these minor issues, the response still conveyed the main points of the legend about St. Hubertus. Therefore, while the response was helpful and mostly aligned with the user’s inquiry, it did not perfectly cater to the user’s needs due to the slight inaccuracies in the translation. So the overall score is 4.
Assistant B	According to legend, St. Hubertus was a rather reckless hunter who was converted and later appointed as the Bishop of Liège after a vision.
Judgment for B	The response provided a translation that was generally accurate and relevant to the user’s request. However, there were slight deviations from the original text. For instance, the term “rather reckless” is less precise than “truly ruthless,” which could lead to some ambiguity. Additionally, the term “Liège” is used instead of “Lüttich,” which is a minor inaccuracy. Despite these minor issues, the response still managed to convey the main points of the original text, making it useful for the user’s needs. Therefore, the response aligns well with the user’s inquiry, with only rare inaccuracies, and thus meets the criteria for a score of 4.